RSC Advances

PAPER

View Article Online
View Journal | View Issue

Cite this: *RSC Adv.*, 2025, **15**, 13111

Coumarin–naphthalene conjugate for rapid optical detection of OCl^- and Y^{3+} in a cascade manner: combined experimental and theoretical studies†

T. Shyam, N. Jahan and D. Das *

Received 29th January 2025
Accepted 10th April 2025

DOI: 10.1039/d5ra00689a

rsc.li/rsc-advances

The coumarin–naphthalene conjugate (**A3**), an ESIPT-active probe, selectively recognized OCl^- in a ratiometric manner in DMSO–water media. The recognition was associated with sky-blue emission (under UV light) as well as yellow emission (under visible light). The OCl^- assisted inhibition of the ESIPT process *via* H-bonding resulted in an intense emission at 484 nm (λ_{ex} = 365 nm). It allowed for the detection of OCl^- as low as 18.42 nM with a strong association constant, $K = 1.08 \times 10^5$ M^{-1}, around physiological pH. Furthermore, the **A3**-OCl^- adduct (**Ad1**) ratiometrically detected Y^{3+} *via* bright orange emission at 556 nm (λ_{ex} = 440 nm) under both UV and visible light. Detection up to 98.51 nM was achieved with a binding constant, $K = 1.38 \times 10^5$ M^{-1}, at physiological pH. Density functional theory (DFT) and lifetime decay measurements substantiated the interactions. Real sample analysis were also achieved with the developed method.

Introduction

Nowadays, the detection and quantification of various environmental and biological contaminants is a primary concern.[1,2] Different types of pollutants, such as cationic, anionic, and molecular species,[3,4] exhibit different types of interactions. Nitrate, fluoride, phosphate, hypochlorite, bromate, arsenate, nitrite, chloride, sulfide, and cyanide are common anionic contaminants. Among them, hypochlorite (OCl^-) is a contaminant frequently encountered due to its application in household bleaching,[5,6] particularly for drinking water disinfection.[7] This facilitates its easy entry into biological systems. Being one of the bio-relevant reactive oxygen species (ROS),[8] OCl^- plays an important role in several natural processes. For example, endogenous OCl^- is generated from the myeloperoxidase (MPO) enzyme-catalyzed reaction between H_2O_2 and Cl^-.[9] It is a powerful *in vivo* oxidant with effective antibacterial activity during microbial invasion.[10] Excess OCl^- is detrimental to various biomolecules, including DNA, RNA, fatty acids, cholesterol, and proteins,[11] and it is also responsible for tissue damage and diseases such as atherosclerosis, arthritis, and cancer.[12–14] It is employed as a safe disinfectant for drinking water and swimming pools. It is also used as a bleaching agent in industrial applications. These are potential external sources of OCl^-.[15] Thus, easy and instant detection, as well as quantification of OCl^-, is highly relevant and in demand.

Yttrium (Y) is a second-row transition metal, but its property similarities with the lanthanides make it unique. It has diverse applications in various fields such as materials, medicine, and catalysis. In the materials industry, synthetic garnets,[16] cathode ray tubes for color televisions,[17] near-IR lasers,[18] white LEDs,[19] spark plugs,[20] superconductors,[21] and material enhancers[22] are some common applications. Y has extensive use in organic catalytic reactions, such as intermolecular aminoalkene hydroamination,[23] *o*-selective C–H addition,[24] lactide polymerization,[25] acylation of alcohols, Diels–Alder reactions,[26] asymmetric hydroamination,[27] and the Tishchenko reaction, among others.[28] In the medicinal field, it is used for the treatment of cancer as a source of powerful β radiation. For example, Y^{90}-DOTA-tyr3-octreotide[29] and Y^{90} ibritumomab tiuxetan[30] are two drugs used to treat various cancers, including lymphoma, leukemia, liver cancer, and bone cancer.

Optical probes, such as colorimetric and fluorescent probes, are very useful and popular due to their selectivity, rapidity, sensitivity, simplicity, direct visual perception, non-invasiveness, and low-cost methodology.[31–36] The literature indicates that most dual probes for assaying OCl^- as one of the analytes suffer from background fluorescence, solvent dependence, and time-consuming synthesis.[37,38] Thus, there is ample scope to contribute to overcoming these limitations. Similarly, the number of optical sensors for Y^{3+} is limited.

These facts led us to design and develop a simple, inexpensive, highly selective probe, **A3**. A simple receptor-linker-fluorophore-type compound (**A3**), where coumarin and naphthalene are connected *via* hydrazine, was developed. This type

Department of Chemistry, The University of Burdwan, Burdwan-713104, WB, India. E-mail: ddas100in@yahoo.com; Fax: +91-342-2530452; Tel: +91-342-2533913 (ext. 424)

† Electronic supplementary information (ESI) available. See DOI: https://doi.org/10.1039/d5ra00689a

of structure was a potential candidate for excited-state intramolecular proton transfer (ESIPT), intramolecular charge transfer (ICT), photo induced electron transfer (PET), chelation-enhanced fluorescence (CHEF), through-bond energy transfer (TBET), chelation-enhanced quenching (CHEQ), and excimer/exciplex formation. The **A3** probe was found to be a fluorescence probe for the trace-level recognition and determination of OCl^- and Y^{3+} in a cascade manner through the ESIPT and CHEF processes in a green solvent system, such as DMSO–water.

Upon interaction with OCl^-, the colorless probe emitted sky-blue fluorescence, turning the solution yellow to the naked eye, allowing the detection of OCl^- as low as 18.42 nM. Subsequent addition of Y^{3+} turned the fluorescence to orange, allowing its detection up to 98.51 nM.

Materials and methods

Synthesis

Synthesis of A3. The 4-carboxymethyl-8-formyl coumarin (**A1**) was prepared following the published method.[39] Then, **A2** was prepared by drop-wise addition of **A1** (202 mg, 0.82 mmol) to hydrazine in a 1 : 1 mole ratio in EtOH with overnight stirring. The resultant product was crystallized and characterized by mass spectrometry (Fig. S1a, ESI†), FTIR (Fig. S1b, ESI†), and ^{1}H-NMR (Fig. S1c and d, ESI†) spectra. Finally, the coumarin–naphthalene conjugate, **A3**, was prepared by refluxing a mixture of **A2** (130 mg, 0.50 mmol) and 2-hydoxy-1-naphthaldehyde (86 mg, 0.50 mmol) in EtOH for 4 h (Scheme 1). The resulting pale yellow solution yielded pure **A3** after a few days *via* crystallization. The **A3** was characterized by different spectroscopic techniques, namely, mass spectrometry (Fig. S2a, ESI†), FTIR (Fig. S2b, ESI†), and ^{1}H-NMR (Fig. S2c and d, ESI†) spectra.

Synthesis of Ad1 (A3-OCl^-) and Ad2 (A3-Y^{3+}) adducts. The ethanol solution of **A3** and OCl^- was mixed under stirring conditions in a 1 : 1 mole ratio. Stirring was continued for 15 min. The resultant mixture was subjected to filtration to remove any suspended particles, and the filtrate was kept undisturbed for slow evaporation of the solvent. After two days, a pale yellow solid was collected and characterized as **Ad1** by spectroscopic techniques such as mass spectrometry (Fig. S3a, ESI†) and FTIR (Fig. S3b, ESI†).

Likewise, **Ad2** was obtained by stirring the mixture of **Ad1** and Y^{3+} (ethanol solution) in a 1 : 1 mole ratio and characterized by mass spectrometry (Fig. S4a, ESI†) and FTIR (Fig. S4b, ESI†) spectra.

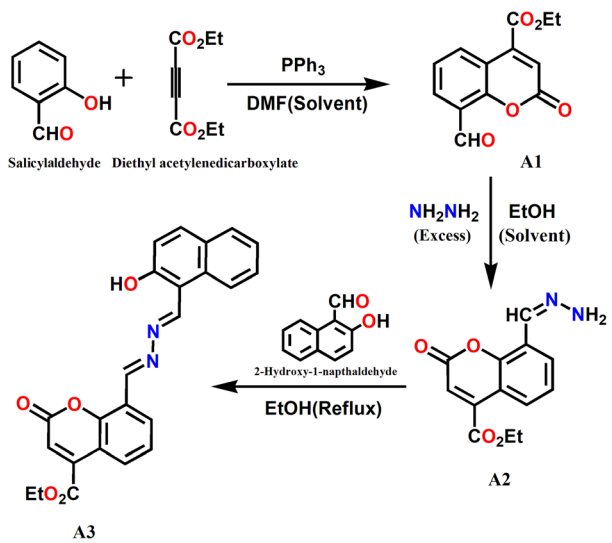

Scheme 1 Synthesis of **A3**.

Results and discussion

The optical response of the probe, **A3**, towards common ROS/RNS (such as O_2, H_2O_2, NO, O^{2-}, OH^-, $ONOO^-$, and ROO^-) and anions (such as F^-, Cl^-, Br^-, I^-, SO_4^{2-}, SO_3^{2-}, $H_2PO_4^-$, ClO_4^-, SCN^-, NO_3^-, NO_2^-, $H_2AsO_4^-$, and BzO^-) was tested. Interestingly, **A3** selectively detected OCl^- in PBS-buffered (10 mM, pH 7.4) DMSO–water (1 : 7) media.

Absorption spectroscopic studies

UV-Vis absorption spectra of **A3** [20 μM] in the presence of common ROS/RNS and anions were recorded (Fig. 1A). Interestingly, only OCl^- significantly changed the spectrum of **A3**. **A3** showed two intense absorption peaks, at 313 nm and 360 nm, along with a relatively weak peak at 413 nm. Upon addition of OCl^- [0–1800 μM], the absorbance at 313 nm and 360 nm decreased, while it increased at 413 nm in a ratiometric manner. The colorless solution turned yellow (Fig. 1B). In contrast, other tested common ROS/RNS and anions did not significantly affect the absorption spectra of **A3**.

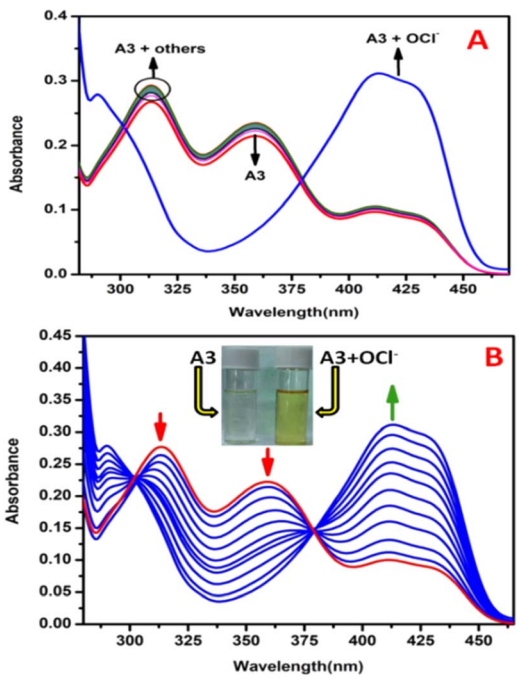

Fig. 1 Changes in the absorption spectra of **A3**: (A) in the presence of common ROS/RNS and anions; (B) with [OCl^-] (media: PBS-buffered DMSO–water (10 mM, 1 : 7, v/v, pH 7.4)).

Emission spectroscopic studies

The emission studies were performed in the same media as mentioned above. **A3** exhibited a weak emission at 394 nm (λ_{ex} = 365 nm). Except for OCl^-, other tested common ROS/RNS and anions did not significantly affect its emission spectra (Fig. 2A). Upon gradual addition of OCl^-, a new emission peak at 484 nm gradually increased, accompanied by intense sky-blue fluorescence (Fig. 2B). Interference studies with different common anions and ROS/RNS (listed above) were performed at varying concentrations. No interference was observed, though (Fig. S5, ESI†). The quantum yields of **A3** in the absence and presence of OCl^- were 0.0164 and 0.1415, respectively. The effect of pH on the emission of **A3**, in the absence and presence of OCl^- was also checked (Fig. S6, ESI†). The change in emission intensity was maximum in the pH range of 6 to 8.5, making it functional at physiological pH 7.4.

The Job's plot showed 1 : 1 (mole ratio) stoichiometry for the **A3**-OCl^- adduct (**Ad1**) (Fig. S7, ESI†). The stoichiometry of the **A3**-OCl^- adduct was also supported by the mass spectrum (Fig. S3a, ESI†). The binding constant of **A3** for OCl^- was determined using the Benesi–Hildebrand[40–43] equation, assuming a 1 : 1 stoichiometry and was found to be 1.08×10^5 M^{-1} (Fig. S8, ESI†). Emission intensities at 484 nm were used to determine the lowest detection limit.[44,45] The limit of detection (LOD) of **A3** for OCl^- was 18.42 nM (Fig. S9, ESI†). The plot of emission intensity of **A3** *vs.* OCl^- was linear up to 21 μM OCl^-, which was useful for measuring unknown OCl^- concentrations

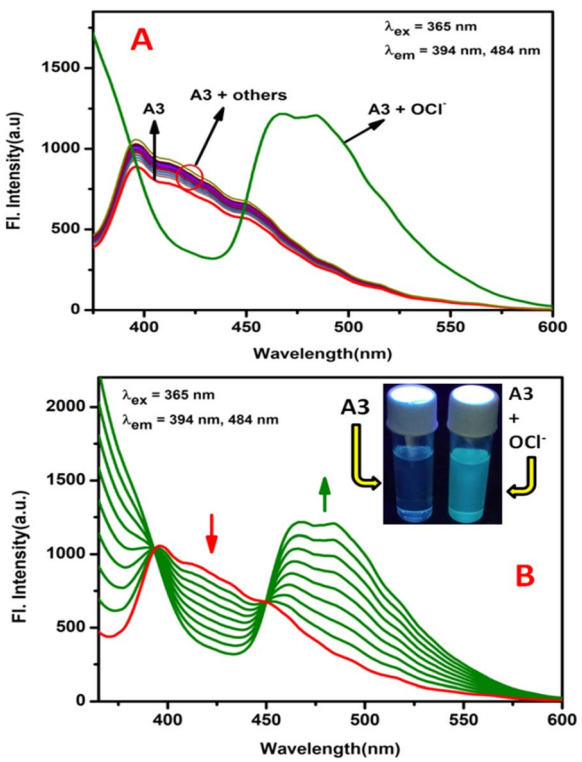

Fig. 2 Changes in the emission spectra of **A3**: (A) upon addition of common ROS/RNS and anions; (B) with [OCl^-]. Media and pH are mentioned above.

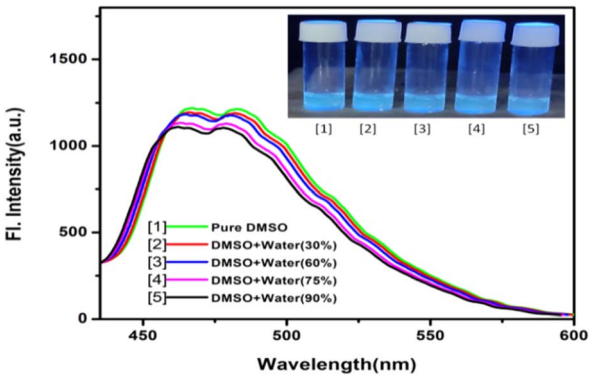

Fig. 3 Emission spectra of **Ad1** in a solvent system with varying percentages of water.

(Fig. S10, ESI†). Addition of water to DMSO slightly lowered the emission maxima with a minute blue shift (Fig. 3).

Sequential recognition of yttrium ion (Y^{3+})

The **Ad1** (**A3**-OCl^-) [20 μM] acted as a proficient candidate for sequentially recognizing yttrium ion (Y^{3+}) ratiometrically by both absorption and emission spectroscopy in the same medium. In response to Y^{3+} ion [0–1800 μM], the **Ad1** altered its emission with a red shift from blue (λ_{em} = 489 nm) to yellowish-orange (λ_{em} = 555 nm), along with a visible color change from yellow to orange (Fig. 4).

The other rare earth cations (such as La^{3+}, Ce^{4+}, Nd^{3+}, Sm^{3+}, Gd^{3+}, and DY^{3+}) along with common cations (such as Na^+, K^+, Ca^{2+}, Mg^{2+}, Ni^{2+}, Al^{3+}, Co^{2+}, Zn^{2+}, Mn^{2+}, Cu^{2+}, Fe^{2+}, Hg^{2+}, and

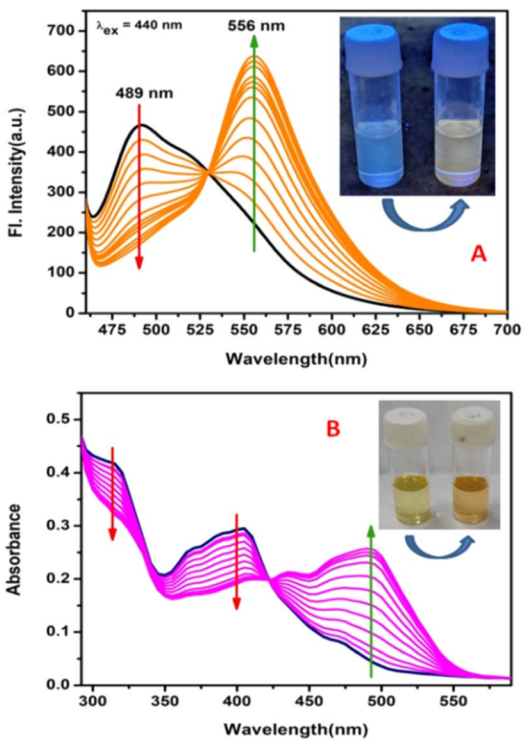

Fig. 4 Changes in (A) emission and (B) absorption spectra of **Ad1** upon addition of Y^{3+}.

Fe^{3+}) remained inert toward **Ad1**. Only Y^{3+} responded selectively (Fig. S11, ESI†). Other tested cations showed negligible interference when tested at different concentrations (Fig. S12, ESI†). The LOD for Y^{3+} was 98.51 nM (Fig. S13–S14, ESI†), with a binding constant of 1.38×10^5 M^{-1} (Fig. S15, ESI†). It functioned well at physiological pH (Fig. S16, ESI†). The quantum yields of **Ad1** and **Ad2** were 0.1415 and 0.536, respectively. The Job's plot showed 1 : 1 (mole ratio) stoichiometry for **Ad2** (Fig. S17, ESI†).

Proposed sensing mechanism

ESIPT active[46] **A3** (Fig. S18, ESI†) contains a –OH moiety *ortho* to the imine group, which easily undergoes tautomerization. Upon addition of OCl^- to **A3**, the ESIPT proton is arrested *via* an H-bond, resulting in fluorescence enhancement (Fig. 5). It is noteworthy that direct interaction between Y^{3+} and **A3** did not lead to fluorescence recognition of Y^{3+}, probably because **A3** failed to chelate Y^{3+}.

However, in the presence of OCl^-, **A3** could recognize Y^{3+} *via* a change in its emission profile. This means the [**A3**+OCl^-] adduct (**Ad1**) acts as a fluorescence sensor for Y^{3+}. This may be due to the fact that OCl^- aids in the deprotonation of the –OH group of **A3**, facilitating chelation to Y^{3+}, which results in a change in its emission profile. Thus, fluorescence recognition of Y^{3+} can be termed as OCl^--assisted CHEF process (Fig. 5). ^{1}H-NMR studies supported the proposed binding interaction (Fig. 6), which was also corroborated by mass (Fig. S3a and S4a, ESI†) and FTIR (Fig. S3b and S4b, ESI†) spectral results. The proposed binding stoichiometry matched that predicted from Job's studies (Fig. S7 and S17, ESI†).

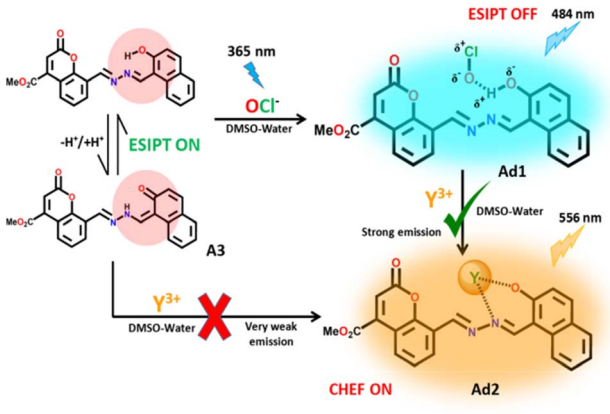

Fig. 5 Proposed binding and sensing mechanism for OCl^- and Y^{3+} by **A3** in a cascade manner.

^{1}H-NMR studies

^{1}H-NMR studies were performed to demonstrate the binding interaction of **A3** with OCl^- and Y^{3+} in a cascade manner. Upon addition of 0.5 equiv. OCl^-, the highly de-shielded phenol –OH proton shifted downfield from 13.158 ppm to 13.615 ppm, while its intensity significantly diminished. Two imine protons also experienced a slight downfield shift from 10.302 ppm and 10.830 ppm to 10.314 ppm and 10.836 ppm, respectively. Addition of 1.0 equiv. OCl^- to **A3** further enhanced the intensity of the phenol proton, along with its downfield shift from 13.615 ppm to 14.014 ppm. In addition, the imine protons further shifted downfield from 10.314 ppm and 10.836 ppm to 10.324 ppm and 10.844 ppm, respectively. All these

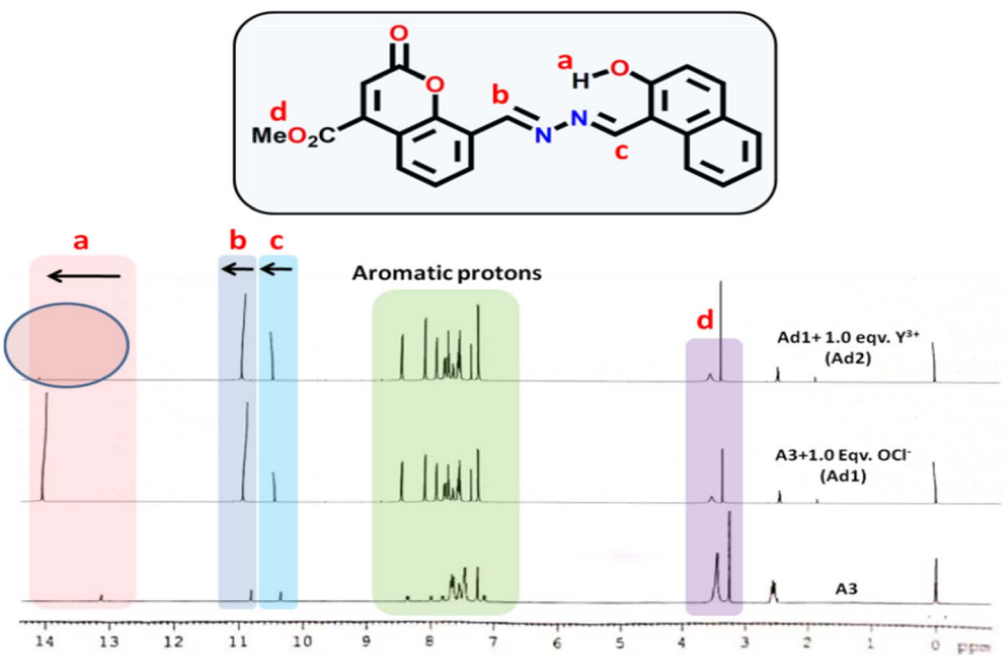

Fig. 6 Changes in the ^{1}H-NMR spectra of **A3** upon addition of OCl^- and Y^{3+} in a cascade manner (solvent, $CDCl_3$).

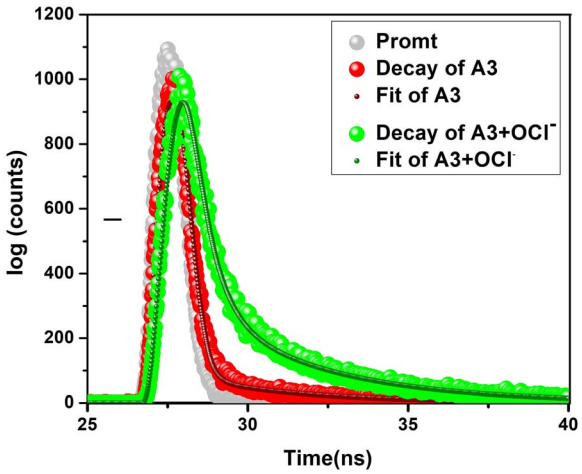

Fig. 7 Fluorescence lifetime decay profile.

observations suggest H-bonding interaction between phenol–OH with OCl^-.

Upon addition of 1.0 equiv. Y^{3+} to the [**A3**+OCl^-] adduct (**Ad1**), the phenol–OH peak disappeared, and the two imine proton peaks further shifted downfield to 10.384 ppm and 10.886 ppm, respectively (Fig. 6). The data is provided in ESI (Table S1).†

Fluorescence life time decay studies

The change in emission characteristics of **A3** in the presence of OCl^- (at 484 nm) was also reflected (IRF 336 nm) in its fluorescence lifetime decay profile (Fig. 7). The average lifetime of **A3** increased from 1.91 ns to 3.78 ns (1.98 times) in the presence of OCl^-, indicating an interaction between **A3** and OCl^-.

DFT studies

TD-SCF/DFT/B3LYP/6-311G level of theory was employed to optimize the energy levels of **A3** and **Ad1**. The lowering of the HOMO–LUMO energy gap from **A3** (0.10093 eV) to **Ad1** (0.09699 eV) indicated an interaction between **A3** and OCl^-, leading to the formation of **Ad1** (Fig. 8). The oscillator strength (f^b) for the $S_0 \rightarrow S_1$ transition increased in **Ad1** ($f = 0.0019$) compared to **A3** ($f = 0.0001$). The oscillator strength (f^b) and transitions involved, along with their energy levels, are listed in Table S2 (ESI).†

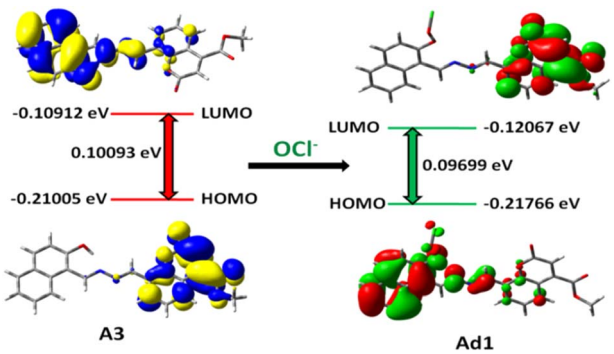

Fig. 8 Frontier molecular orbitals of A3 and its adduct Ad1.

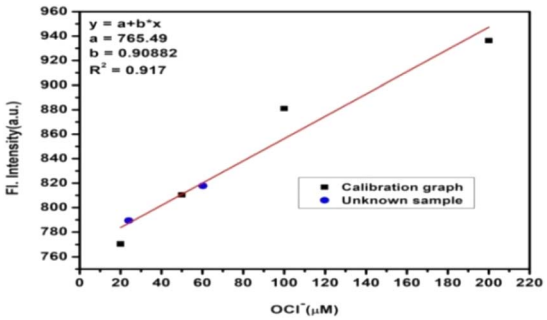

Fig. 9 Calibration graph for the determination of unknown [OCl^-].

Application

Real sample analysis for OCl^-

Water samples collected from local source were analyzed to determine OCl^- concentration employing **A3**, following the standard addition method.[47] The concentration was measured utilizing the calibration plot, which involved the emission intensity of **A3** *vs.* [OCl^-].

For this purpose, 0.1 mL of a 4×10^{-4} M solution of **A3** in DMSO was mixed with 1 mL of the unknown water sample, and the volume was adjusted to 4 mL such that the final solution had the composition DMSO : water, 1 : 7 (v/v). Similarly, four known OCl^- solutions with concentrations of 20 μM, 50 μM, 100 μM, and 200 μM were prepared. Emission intensities of both known and unknown solutions were measured. The concentration of the unknown solution was then calculated from the calibration graph, which was found to be 57.44 μM (Fig. 9).

Real sample analysis for Y^{3+}

The **Ad1** was successfully applied to determine the concentration of Y^{3+} in real water samples following the standard addition method.[45] For this purpose, a known amount of Y^{3+} (as nitrate salt) was added to the collected water samples, namely, river (*R*) and tap (*T*) water from the Durgapur–Asansol industrial area (West Bengal). The total Y^{3+} concentration was then measured using the calibration graph (Fig. S19, ESI†). The following results (Table 1) indicate the efficiency of the developed method.

Comparison of A3 with reported pioneering probes

The efficiency of **A3** was compared with reported pioneering probes (Table 2). The facile synthesis, instantaneous response,

Table 1 Real sample analysis for Y^{3+} concentration

Water sample	Added (10^{-2} M)	Found (10^{-2} M)	Recovery (%)
R1	5.20	4.93	94.23 ± 1.38
R2	10.25	9.81	95.71 ± 1.13
R3	15.10	14.64	96.95 ± 1.06
T1	5.15	4.87	94.56 ± 1.41
T2	10.35	9.9	96.13 ± 1.36
T3	15.22	14.85	97.57 ± 1.05

Table 2 Comparison of **A3** with reported pioneering probes

Sl. No.	System (probe)	Type	Limit of detection (LOD)	Ref.
1	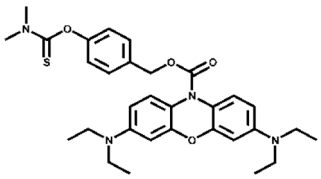	Fluorescence sensor	15.3×10^{-9} M (for OCl^-)	48
2	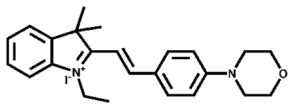	Fluorescence sensor	$5 \times 10–^{8}$ M (for OCl^-)	49
3	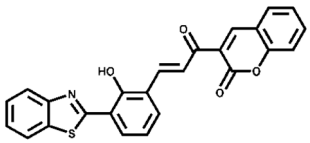	Fluorescence sensor	1.41×10^{-7} M (for OCl^-)	50
4	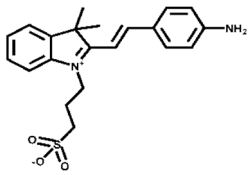	Fluorescence sensor	1.10×10^{-7} M (for OCl^-)	51
5	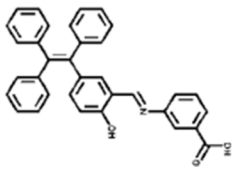	Fluorescence sensor	2.23×10^{-7} M (for Y^{3+})	52
6	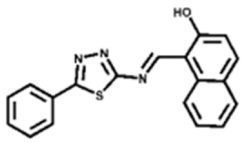	Fluorescence sensor	3×10^{-7} M (for Y^{3+})	53
7	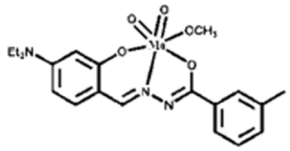	Fluorescence sensor	5.5×10^{-7} M (for Y^{3+})	54
8	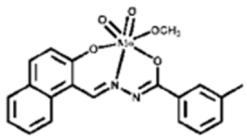	Fluorescence sensor	8×10^{-7} M (for Y^{3+})	54
9	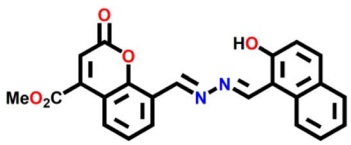	Fluorescence sensor	18.4×10^{-9} M (for OCl^-) 98.5×10^{-9} M (for Y^{3+})	This work

low detection limit, and prompt visualization of both a cation and an anion in a cascade manner make **A3** a very useful probe for practical applications.

Conclusion

The coumarin–naphthalene conjugate (**A3**) is a potential ESIPT-active ratiometric probe for the selective recognition of OCl^-

and Y^{3+} in a cascade manner, with strong sky-blue emission at 484 nm (λ_{ex} = 365 nm) and orange emission at 556 nm (λ_{ex} = 440 nm), respectively. The probe was characterized by FTIR, ESI-MS, and ^{1}H-NMR spectra. The LODs for OCl^- and Y^{3+} were 18.42 nM and 98.51 nM, respectively. The corresponding binding constants were 1.08×10^5 M^{-1} and 1.38×10^5 M^{-1}, respectively. The interference from other common tested analytes was insignificant. Both DFT studies and lifetime decay studies substantiated these interactions.

Data availability

Please note that all data related to the above-mentioned manuscript are available and can be shared upon request. All related data are available in the ESI,† in addition to the main text.

Conflicts of interest

There are no conflicts to declare.

Acknowledgements

We are grateful to Dr I. Ansary of our department for helpful discussions and suggestions.

Notes and references

1 S. D. Richardson and T. A. Ternes, *Anal. Chem.*, 2014, **86**, 2813–2848.
2 J. Zhu, S. Liu, Z. Liu, Y. Li, M. Qiao and X. Hu, *RSC Adv.*, 2014, **4**, 5990–5994.
3 M. Thakur, A. Singh, A. Dubey, A. K. Sundramoorthy, P. Kumar and S. Arya, *Emergent Mater.*, 2024, **7**, 1805–1817.
4 B. Padha, Z. Ahmed, S. Dutta, A. Pandey, N. Padha, M. Tomar, A. Sharma, I. Yadav and S. Arya, *J. Alloys Compd.*, 2025, **1010**, 177673.
5 A. Dutta and W. P. Saunders, *J. Endod.*, 2012, **38**, 1395–1398.
6 J. Park, H. Kim, Y. Choi and Y. Kim, *Analyst*, 2013, **138**, 3368–3371.
7 J. Zhang and X. R. Yang, *Analyst*, 2013, **138**, 434–437.
8 K. Setsukinai, Y. Urano, K. Kakinuma, H. J. Majima and T. Nagano, *J. Biol. Chem.*, 2003, **278**, 3170–3175.
9 A. Hammer, G. Desoye, G. Dohr, W. Sattler and E. Malle, *Lab. Invest.*, 2001, **81**, 543–554.
10 K. Cui, D. Q. Zhang, G. X. Zhang and D. B. Zhu, *Tetrahedron Lett.*, 2010, **51**, 6052–6055.
11 S. Goswami, S. Das, K. Aich, P. K. Nandi, K. Ghoshal, C. K. Quah, M. Bhattacharyya, H. K. Fun and H. A. Abdel-Aziz, *RSC Adv.*, 2014, **4**, 24881–24886.
12 Y. K. Yang, H. J. Cho, J. Lee, I. Shin and J. Tae, *Org. Lett.*, 2009, **11**, 859–861.
13 S. M. Wu and S. V. Pizzo, *Arch. Biochem. Biophys.*, 2001, **391**, 119–126.
14 N. R. Stanley, D. I. Pattison and C. L. Hawkins, *Chem. Res. Toxicol.*, 2010, **23**, 1293–1302.
15 Y. Wang, X. C. Xia, J. Han, X. Bao, Y. Y. Li, X. Tang, L. Ni, L. Wang and M. M. Gao, *Talanta*, 2016, **161**, 847–853.
16 R. Fopase, V. Saxena, P. Seal, J. P. Borah and L. M. Pandey, *Mater. Sci. Eng., C*, 2020, **116**, 111163.
17 V. Innocenzi, I. De Michelis, F. Ferella and F. Vegliò, *Waste Manage.*, 2013, **33**, 2390–2396.
18 J. S. Slimi, H. Yu, H. Zhang, C. Kränkel, P. Loiko, R. M. Solé, M. Aguiló, F. Díaz, W. Chen, U. Griebner, V. Petrov and X. Mateos, *Opt. Express*, 2025, **33**, 2529–2541.
19 M. Kottaisamy, P. Thiyagarajan, J. Mishra and M. S. Ramachandra Rao, *Mater. Res. Bull.*, 2008, **43**, 1657–1663.
20 F. Bisetto, J. Toniolo and R. Menezes, *SAE Technical paper*, 2006, 2006-01–2630.
21 H. Liu, I. I. Naumov, R. Hoffmann, N. W. Ashcroft and R. J. Hemley, *Proc. Natl. Acad. Sci. U. S. A.*, 2017, **114**, 6990–6995.
22 H. J. Lee, K. P. Kim, G. Y. Hong and J. S. Yoo, *J. Lumin.*, 2010, **130**, 941–946.
23 S. Tobisch, *Dalton Trans.*, 2012, **41**, 9182–9191.
24 G. Song, G. Luo, J. Oyamada, Y. Luo and Z. Hou, *Chem. Sci.*, 2016, **7**, 5265–5270.
25 D. Patel, S. T. Liddle, S. A. Mungur, M. Rodden, A. J. Blake and P. L. Arnold, *Chem. Commun.*, 2006, 1124–1126.
26 A. Keshavaraja, V. R. Hegde, B. Pandey, A. V. Ramaswamy, P. Kumar and T. Ravindranathan, *Angew. Chem.*, 1995, **34**, 2143–2145.
27 J. Hannedouche, I. Aillaud, J. Collin, E. Schulz and A. Trifonov, *Chem. Commun.*, 2008, 3552–3554.
28 M. R. Bürgstein, H. Berberich and P. W. Roesky, *Chem.–Eur. J.*, 2001, **7**, 3078–3085.
29 F. Bertagna, R. Giubbini, G. Savelli, C. Pizzocaro, C. Rodella, G. Biasiotto, S. Lucchini, R. Maroldi, J. Rosenbaum and A. Alavi, *Hell. J. Nucl. Med.*, 2009, **12**, 161–164.
30 T. E. Witzig, *Drugs Today*, 2004, **40**, 111.
31 L. Yuan, W. Y. Lin, Y. N. Xie, B. Chen and J. Z. Song, *Chem.–Eur. J.*, 2012, **18**, 2700–2706.
32 J. Deng, P. Yu, Y. Wang and L. Mao, *Anal. Chem.*, 2015, **87**, 3080–3086.
33 Z. Yao, H. Bai, C. Li and G. Shi, *Chem. Commun.*, 2011, **47**, 7431–7433.
34 D. Tan, X. He, X. Xing, Y. Zhao, H. Tang and D. Pang, *Talanta*, 2013, **113**, 26–30.
35 V. V. Kumar and S. P. Anthony, *RSC Adv.*, 2014, **4**, 18467–18472.
36 M. Banerjee, S. Ta, M. Ghosh, A. Ghosh and D. Das, *ACS Omega*, 2019, **4**, 10877–10890.
37 C. Li, Y. Zhou, Y. Li, X. Kong, C. Zou and C. Weng, *Anal. Chim. Acta*, 2013, **774**, 79–84.
38 J. Zha, B. Fu, C. Qin, L. Zeng and X. Hu, *RSC Adv.*, 2014, **4**, 43110–43113.
39 K. C. Majumdar, I. Ansary, S. Samanta and B. Roy, *Synlett*, 2011, **5**, 694–698.
40 H. A. Benesi and J. H. Hildebrand, *J. Am. Chem. Soc.*, 1949, **71**, 2703–2707.

41 A. Banerjee, A. Sahana, S. Das, S. Lohar, S. Guha, B. Sarkar, S. K. Mukhopadhyay, A. K. Mukherjee and D. Das, *Analyst*, 2012, **137**, 2166–2175.
42 S. Das, A. Sahana, A. Banerjee, S. Lohar, D. A. Safin, M. G. Babashkina, M. Bolte, Y. Garcia, I. Hauli, S. K. Mukhopadhyay and D. Das, *Dalton Trans.*, 2013, **42**, 4757–4763.
43 S. Das, S. Lohar, J. S. Matalobos and D. Das, *Chin. J. Chem.*, 2015, **33**, 1173–1177.
44 D. Karak, S. Das, S. Lohar, A. Banerjee, A. Sahana, I. Hauli, S. K. Mukhopadhyay, D. A. Safin, M. G. Babashkina, M. Bolte, Y. Garcia and D. Das, *Dalton Trans.*, 2013, **42**, 6708–6715.
45 S. Ta, S. Das, M. Ghosh, M. Banerjee, S. K. Hira, P. P. Manna and D. Das, *Spectrochim. Acta. A. Mol. Bimol. Spectrosc.*, 2019, **209**, 170–185.
46 H. Guan, A. Zhang, P. Li, L. Xia and F. Guo, *ACS Omega*, 2019, **4**, 9113–9119.
47 M. Ghosh, S. Ta, M. Banerjee and D. Das, *ACS Omega*, 2018, **3**, 16089–16098.
48 M. Q. Zhang, W. H. Guan, J. Wang, B. Zhao, J. Y. Zeng, J. C. Lu, M. Gao and X. B. Wang, *Spectrochim. Acta. A. Mol. Bimol. Spectrosc.*, 2025, **330**, 125738.
49 X. Zhong, L. Zhou, C. Jin, B. Wang, Y. Jiang and J. Shen, *Talanta*, 2019, **202**, 369–374.
50 F. Yan, X. Sun, Y. Jiang, R. Wang, Y. Zhang and Y. Cui, *Dyes Pigm.*, 2020, **182**, 108531.
51 Z. Ma, X. Wang, C. Wang, X. Chen and Q. Lv, *Spectrochim. Acta. A. Mol. Bimol. Spectrosc.*, 2019, **213**, 370–374.
52 S. Jiang, S. Chen, H. Guo and F. Yang, *Dyes Pigm.*, 2020, **183**, 108717.
53 Y. Qin, Q. Meng, J. Yao, M. Chen, Y. Dong, D. Chen, S. He, C. Bai, L. Zhang, B. Wei, H. Miao, C. Qu and R. Qiao, *J. Fluoresc.*, 2023, **33**, 731–737.
54 S. Chatterjee, S. Ta, S. Khanra and D. Das, *RSC Adv.*, 2022, **12**, 33293–33303.